

# Field Effect Induced Organ Distension (FOrge) Features Predicting Biochemical Recurrence from Pre-treatment Prostate MRI

Soumya Ghose<sup>1</sup>(✉), Rakesh Shiradkar<sup>1</sup>, Mirabela Rusu<sup>6</sup>, Jhimli Mitra<sup>1,3</sup>,  
Rajat Thawani<sup>1</sup>, Michael Feldman<sup>4</sup>, Amar Gupta<sup>2</sup>, Andrei Purysko<sup>2</sup>,  
Lee Ponsky<sup>5</sup>, and Anant Madabhushi<sup>1</sup>

<sup>1</sup> Department of Biomedical Engineering,  
Case Western Reserve University, Cleveland, OH, USA  
[sxg709@case.edu](mailto:sxg709@case.edu)

<sup>2</sup> Diagnostic Radiology, Cleveland Clinic Foundation, Cleveland, OH, USA

<sup>3</sup> GE Global Research, Niskayuna, NY, USA

<sup>4</sup> Perelman School of Medicine, University of Pennsylvania, Philadelphia, PA, USA

<sup>5</sup> Department of Urology, Case Western Reserve University School of Medicine,  
Cleveland, OH, USA

<sup>6</sup> Department of Biomedical Engineering, Case Western Reserve University,  
GE Global Research, Niskayuna, NY, USA

**Abstract.** Aggressive cancers are known to induce field effect that affect large areas of cells at a tissue surface. This means that local deformation induced by the tumor as it grows could cause distensions in regions distant from the tumor, presumably even the surface of the organ within which the tumor is growing. In this work, we focused on evaluating whether more and less aggressive prostate cancers (i.e. tumors that subsequently resulted in disease recurrence or not) could differentially induce changes and distensions in the surface of the prostate capsule. Specifically we have developed the concept of a new imaging marker called FOrge features, that attempts to quantify the degree and nature of the deformation induced in the capsule surface on account of tumor growth and then sought to evaluate whether FOrge is predictive of the risk of biochemical recurrence in prostate cancer patients based off a pre-operative T2w

---

Research reported in this publication was supported by the National Cancer Institute of the National Institutes of Health under award numbers 1U24CA199374-01, R01CA202752-01A1, R01CA208236-01A1, R21CA179327-01, R21CA195152-01. The National Institute of Diabetes and Digestive and Kidney Diseases under award number R01DK098503-02. National Center for Research Resources under award number 1 C06 RR12463-01, the DOD Prostate Cancer Synergistic Idea Development Award (PC120857); the DOD Lung Cancer Idea Development New Investigator Award (LC130463); the DOD Prostate Cancer Idea Development Award; the DOD Peer Reviewed Cancer Research Program W81XWH-16-1-0329, the Case Comprehensive Cancer Center Pilot Grant VelaSano Grant from the Cleveland Clinic, the Wallace H. Coulter Foundation Program at Case Western Reserve University. The content is solely the responsibility of the authors and does not necessarily represent the official views of the National Institute of Health.

MRI scan. The FOrgE features were extracted from a spatially contextual surface of interest (SOI) of the prostate capsule, uniquely determined from statistically significant shape differences between prostate atlases constructed from patients who did (BCR+) and who did not (BCR-) undergo biochemical recurrence. A random forest classifier trained on the FOrgE features extracted from atlas images (25 BCR+ and 25 BCR-) yielded an accuracy of 78% and an AUC of 0.72 in an independent validation set of 30 patients.

## 1 Introduction

Field cancerization or field effect is often observed in aggressive cancers that affects tissues far beyond the tumor periphery due to genetic and/or epigenetic alterations. Such alterations are often strongly associated with local recurrence of various kinds of cancer including prostate. Biochemical recurrence (BCR), which is defined as an elevated prostate specific antigen (PSA) of 0.2 ng/ml for surgery or 2 ng/ml for radiation therapy above the nadir, is strongly suggestive of disease recurrence and hence treatment failure in prostate cancer patients who have undergone definitive therapy. BCR is typically associated with aggressive cancer growth that may induce field effect and deform the prostate capsule resulting in an irregular bulge and/or focal capsular retraction.

Previous work for prostate cancer detection, risk stratification and recurrence prediction has focused on using image texture features of the tumor and radiomic characterisation of the prostate [1,2]. However the cancer field effect that is strongly correlated to disease recurrence and that may mechanically deform prostate capsule surface far beyond the tumor periphery has not, thus far, been computationally investigated. To the best of our knowledge, no other studies have investigated the distil mechanical effect of the growth of an aggressive recurring tumour on the prostate surface, with a view to predicting outcome.

We hypothesize that such differential localized deformation of the prostate SOI may arise from the field effect of aggressive growth of the confined tumour for BCR+ patients. We quantify such localized deformation with deformation magnitude and orientation features to discriminate BCR+ and BCR- patients.

In this work we present FOrgE features extracted from a spatially contextual SOI of the prostate capsule that quantifies prostate capsule deformation magnitude and orientation to predict prognosis of recurrence. There are two major contributions of this work;

- A new set of 3D shape features that captures subtle cues with regard to the prostate capsule surface deformations was developed.
- The FOrgE features were extracted from a spatially contextual surface of interest (SOI) of the prostate capsule, uniquely determined from statistically significant shape differences of BCR+ and BCR- atlases to predict BCR.

The closest work in literature compared to our work is that of Rusu et al. [3]. Rusu et al. showed that statistically significantly difference in the prostate capsule shape exist between patients with and without cancer. Unlike Rusu et al.,

our work is however focused on BCR. More importantly Rusu et al. have not translated their observation to a shape based descriptor for classification or prediction of disease outcome. In our work however we evaluate FORge features for the task of prediction of recurrence of prostate cancer. Even though the FORge features are used in prediction of recurrence of prostate cancer, the concept may be extended to aggressive cancer prediction of other organs like the breast, kidney, bladder and the lung.

## 2 Methods

### 2.1 Brief Overview

The BCR prediction method may be broadly be divided into three parts, (1) Creation of BCR+ and BCR- cohort atlases, (2) Identification of the surface of interest (SOI) that significantly differs between BCR+ and BCR- atlases and (2) Extraction of FORge features from SOI to predict BCR patients in a validation set. The entire framework is presented in Fig. 1.

### 2.2 Creation of BCR+ and BCR- Cohort Atlases

Spatially contextual SOI of the prostate capsule was uniquely identified from a statistical significant shape differences between BCR+ and BCR- atlases created from the training images. The prostate with median volume of each cohort

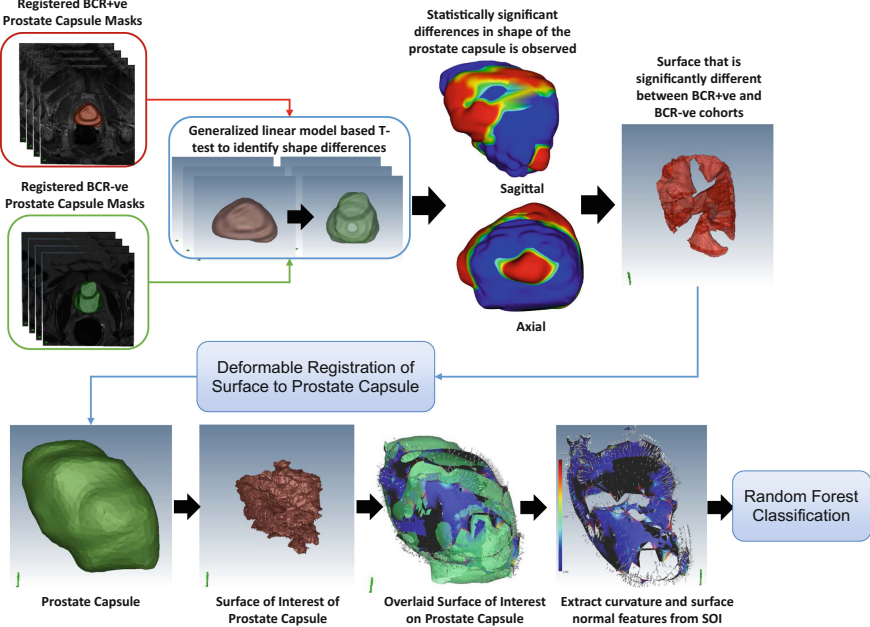


Fig. 1. Biochemical recurrence prediction framework

was selected as the representative template for the cohort. The remaining T2w images of each of the cohorts were registered to the representative template to create BCR+ and BCR− atlases given by A+ and A− respectively.

A block matching strategy described in [4] was adopted to determine the transformation parameters for the affine registration. Similarity between a block from the moving image to all blocks of similar dimension in the fixed or the reference image was computed. The best corresponding block defined the displacement vector for the affine transformation. Normalized cross correlation based similarity was used to determine the block correspondences. The affine registration of the moving image to the reference image was followed with a B-spline [5] based non-rigid registration. Segmented prostate masks were used to constrain the registration in the volume of interest. The manually segmented masks of the prostate capsules were given the same transformation as the registered images to bring the prostate masks/surfaces in correspondence.

### 2.3 Spatially Contextual Surface of Interest (SOI)

To perform a statistical comparison of the prostate capsule shape between BCR+ and BCR− patients, atlas A+ created for BCR+ patients were registered to atlas A− of the BCR− patients. All registered prostate capsules of both the BCR+ and BCR− groups were isotropically scaled to  $0.3\text{mm}^3$  resolution and transformed into signed distance function. The signed distance representation gives an implicit representation of the prostate boundary and aids in a t-test based comparison of the shape in a non-parametric General Linear Model (GLM) based t-test framework [6]. Statistically significant shape differences were quantified with 5000 random permutation testing with the p-value being corrected for multiple comparison. A voxel was considered as belonging to a region exhibiting statistically significant differences between shapes for BCR+ and BCR− patients if the p-value estimated by this extensive testing was less than 0.05. Significant shape differences between BCR+ and BCR− cohorts were then quantified as SOI. The entire framework for statistical shape differences quantification is presented in Fig. 1.

### 2.4 Field Effect Induced Organ Distension (FOrge) Features

To quantify the irregular deformation of the prostate capsule in SOI, curvature magnitude and surface normal orientation features were extracted. The surface curvature and orientation features were however meaningful in spatially contextual SOI which is significantly different between the BCR+ and BCR− cohorts. To extract the curvature and surface orientation features from spatially contextual SOI, all patients were rigidly registered to the BCR− template selected for statistical comparison of BCR+ and BCR− cohorts. The SOI mask identified via population based statistical comparison (as explained in Sect. 2.2) was then registered to patient mask using a B-spline based registration. This ensures that the patient mask was not deformed and remains un-affected. The registered mask was then considered as the SOI for the patient for feature extraction.

The surface normal orientation reflects the direction of the surface deformation and the surface Gaussian curvature reflects corresponding magnitude. Gaussian curvature and normal orientation features were extracted for every vertex of the mesh.  $K^{th}$  Gaussian curvature discretized at vertex  $v$  was given by,

$$K_v = 2 \times PI - \sum_{\nabla} (v_\gamma) \quad (1)$$

where  $\sum_{\nabla}$  is the summation of all facets and  $v_\gamma$  is the orientation at  $v$ . For every vertex normal orientation was represented in spherical coordinate system and  $\theta$  the angle between the projection of the normal vector in  $XY$  plane and  $X$  axis and  $\phi$  the angle between the projection of the normal vector in  $YZ$  plane and  $Z$  axis were extracted.

For every patient three arrays of curvature,  $\theta$  and  $\phi$  were created and statistical measures like mean, standard deviation, inter-quartile range (Q1 and Q3), range, skewness and kurtosis were extracted. Thus the dimension of feature vector for every patient was 21, coming from three features (curvature,  $\theta$  and  $\phi$ ) and seven statistical measures (mean, standard deviation, inter-quartile range (Q1 and Q3), range, skewness and kurtosis) for each of the three features.

### 3 Experimental Results and Discussions

#### 3.1 Data Description and Preprocessing

In this single center Institutional Review Board (IRB) approved study 874 patients were selected from a prostate MRI registry. Availability of complete image datasets (T1w, T2w and ADC maps), no treatment for PCa before MRI; presence of clinically localized PCa; Gleason score available from pretreatment biopsy and/or from radical prostatectomy specimens; and post-treatment outcome data including post-treatment PSA and a minimum of 3 years of follow-up were used as inclusion criteria. Of the 874 patients in the registry, 80 cases met these criteria. BCR+ and BCR- cases for atlas creation were selected from these 80 patients. To reduce statistical biases of the atlases, an equal number of patients in the BCR+ and BCR- cohorts (25 each); similar Gleason scores (6 to 9); and similar tumor stages (T2 to T3) were used to identify 50 patients. The remaining 30 patients out of 80 were used for validation. The BCR+ patients had a mean recurrence time of 18.5 months. The BCR- patients had a mean follow-up time of 4.2 years. An experienced genitourinary radiologist with more than 7 years of experience in reading prostate MRI reviewed the T1 and T2w images before manually contouring the prostate gland on T2-weighted images. Prior to performing the FOrge analysis, N4 bias field correction [7] was applied to all T2w images.

#### 3.2 Evaluation of Atlas Construction

The population based statistics used to identify spatially contextual SOI that significantly differs between the two cohorts is however dependent on the quality

of the registration of the atlases A+ and A-. The A+ and A- atlases registration accuracy was evaluated in terms of Dice similarity coefficient (DSC) and mean absolute surface distance (MASD). The DSC of A+ atlas was  $0.98 \pm 0.01$  and that of A- was  $0.97 \pm 0.01$ . The MASD of A+ atlas was  $0.30 \pm 0.11$  mm and that of A- atlas was  $0.40 \pm 0.14$  mm. The registration accuracy for atlas creation may suggest that the atlases were created sufficiently accurately for statistical shape comparison.

### 3.3 Evaluation of FOrgE Features from SOI vs Entire Capsule

The accuracy of FOrgE features extracted from SOI are compared to the FOrgE features extracted from the entire mesh using a random forest (RF) classifier. This is done to highlight the importance of extracting features from targeted spatially constrained SOI that significantly differs between the two population cohorts. The results are presented in Fig. 2.

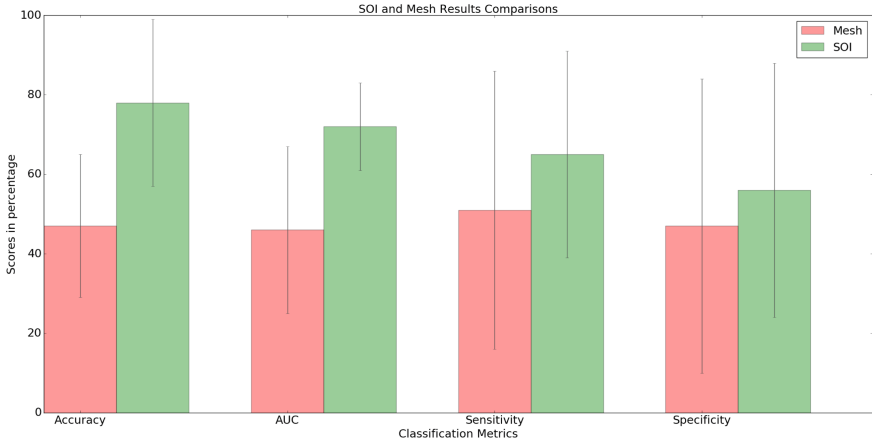


**Fig. 2.** Comparison of classification accuracy between FOrgE features extracted from entire mesh and constrained SOI on the independent test set ( $n = 30$ ).

The performance of a RF classifier trained on FOrgE features from SOI compared to the entire mesh is significantly better ( $p < 0.05$ ) for accuracy, AUC, sensitivity and specificity as observed in Fig. 2. This may suggest that to discriminate BCR+ and BCR- population it is important to extract curvature and normal features from targeted spatially contextual SOI.

The depth of the RF classifier was fixed to 2 and 10,000 trees were used to prevent over fitting. RF Gini impurity index were then used to identify top performing features from the training data (25 BCR+ and 25 BCR-). The feature dimension was then reduced to top 9 features to prevent over fitting and improve accuracy. We used the RF Gini impurity score for feature selection as

the feature distributions were not Gaussian and a non-parametric multi-variate feature selection model was necessary. Most traditional feature selection methods cannot account for both non-parametric and multivariate feature selection simultaneously unlike RF Gini impurity score. The Gini importance score for the top 9 features are presented in Table 1. The figure showing the difference in  $\phi$  distribution between BCR+ and BCR- patients is presented in Fig. 3.

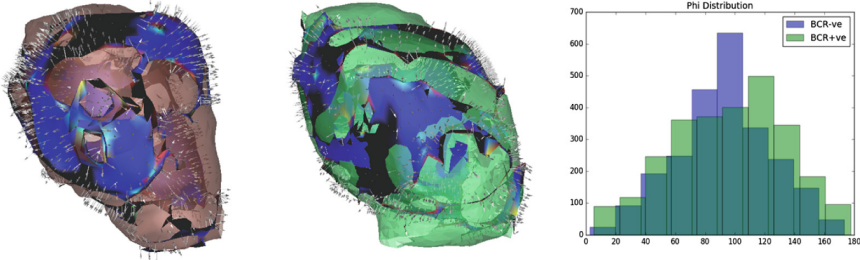


**Fig. 3.** BCR+ve and BCR-ve patients exhibits differential  $\phi$  distribution in the SOI. The left panel shows the SOI overlaid on a BCR+ve and middle panel shows the SOI overlaid on a BCR-ve prostate cancer patients. The rightmost panel shows the overlay of the  $\phi$  feature distribution between BCR+ve and BCR-ve SOI.

**Table 1.** Gini importance score for top 9 features. Abbreviations used std = standard deviation, Curv = curvature, krt = kurtosis

	$\phi$ std	Curv std	Curv range	Curv mean	$\theta$ mean	$\theta$ krt	$\theta$ range	$\phi$ range	$\theta$ std
Gini score	0.090	0.079	0.072	0.071	0.067	0.056	0.055	0.046	0.043

As every tree in RF selects  $\sqrt{\text{features}}$ , fixing feature dimension to 9 ensured that every tree in RF would have three features which in turn ensured that every tree can grow to a depth of 2. A three-cross validation over the training set resulted in an accuracy of  $0.80 \pm 0.21$  and an AUC of  $0.72 \pm 0.11$ . Eventually the entire training dataset is then used to build the classifier for the validation set of 30 patients and the results are presented in Fig. 2. The RF classifier using the FORge features yielded an AUC=0.72 and an accuracy of  $0.78 \pm 0.21$  on the test set ( $n = 30$ ).

## 4 Conclusions

In this work we presented a new spatially contextual discriminative (FORge) shape features that captures prostate capsule deformation magnitude and orientation in a SOI for predicting BCR. We have also shown that FORge extracted

from the entire prostate mesh had a significantly inferior performance compared to a spatially localized region which was found to be significantly different between the BCR+ and BCR− population cohorts.

We acknowledge that our study did have its limitations. As described in the approach, the FOrge features are only predictive when extracted within the SOI regions identified on the prostate surface. In other words, the precise identification of the SOI is a critical step to ensure success of the approach. Clearly we need to address the sensitivity of our features to changes in location and contour of the SOI in future work. Additionally, we did not explicitly control for peripheral and central gland tumors in this study. It is not clear whether the FOrge features might be more or less predictive based off the geographical location of the tumor in the prostate.

Another avenue for future research is to integrate a more traditional tumor radiomics approach with the FOrge features to assess whether the combination results in improved predictive performance compared to either approach individually. Finally, a multi-site validation of the approach on a larger independent cohort is needed to confirm the preliminary findings presented in this work.

## References

1. Hegde, J.V., Mulkern, R.V., Panych, L.P., Fennessy, F.M., Fedorov, A., Maier, S.E., Tempany, C.M.: Multiparametric MRI of prostate cancer: an update on state-of-the-art techniques and their performance in detecting and localizing prostate cancer. *J. Magn. Reson. Imaging* **37**(5), 1035–1054 (2013)
2. Gnep, K., Fargeas, A., Gutierrez-Carvajal, R.E., Commandeur, F., Mathieu, R., Ospina, J.D., Rolland, Y., Rohou, T., Vincendeau, S., Hatt, M., Acosta, O., de Crevoisier, R.: Haralick textural features on T2-weighted MRI are associated with biochemical recurrence following radiotherapy for peripheral zone prostate cancer. *J. Magn. Reson. Imaging* **45**(1), 103–117 (2017)
3. Rusu, M., Puryrsko, A.S., Verma, S., Kiechle, J., Gollamudi, J., Ghose, S., Herrmann, K., Gulani, V., Paspulati, R., Ponsky, L., Bohm, M., Haynes, A.M., Moses, D., Shnier, R., Delprado, W., Thompson, J., Stricker, P., Madabhushi, A.: Computational imaging reveals shape differences between normal and malignant prostates on MRI. *Sci. Rep.* **7**, 41261 (2017)
4. Ourselin, S., Roche, A., Subsol, G., Pennec, X., Ayache, N.: Reconstructing a 3D structure from serial histological sections. *Image Vis. Comput.* **19**(1), 25–31 (2001)
5. Rueckert, D., Sonoda, L.I., Hayes, C., Hill, D.L., Leach, M.O., Hawkes, D.J.: Non-rigid registration using free-form deformations: application to breast mr images. *IEEE Trans. Med. Imaging* **18**(8), 712–721 (1999)
6. Winkler, A.M., Ridgway, G.R., Webster, M.A., Smith, S.M., Nichols, T.E.: Permutation inference for the general linear model. *Neuroimage* **92**, 381–397 (2014)
7. Tustison, N.J., Avants, B.B., Cook, P.A., Zheng, Y., Egan, A., Yushkevich, P.A., Gee, J.C.: N4ITK: improved N3 bias correction. *IEEE Trans. Med. Imaging* **29**(6), 1310–1320 (2010)